

Beating The Limits of Noise

Week

VIII

The Laser Interferometer Gravitational-Wave Observatory (LIGO) stands as one of the most impressive examples of optical interferometric sensing. As we will see, LIGO builds upon a very simple Michelson interferometer design, enhanced with a few additional components, tweaks, and ideas in the realm of optical interferometric sensing that we already discussed in our course. These enhancements are designed to match the capabilities of the equipment to the requirements of the problem, being able to detect minuscule ripples in spacetime caused by gravitational waves, with arm lengths extending four kilometers to maximize sensitivity.

For the next two weeks, and leveraging such extreme operation conditions and required sensitivities, we will focus on the LIGO as a case study to discuss the **role of noise when extreme precision is required**, showing that even in ideal conditions, the quantum nature of physics adds a certain noise limit - the **standard quantum limit**. We will discuss the origin and role of quantum noise in LIGO interferometric sensors, and how we can tame it when we need precise measurements utilizing a quantum-related tool, the vacuum **squeezed states**.

1 The Origin of Gravitational waves

In very generic terms, gravitational waves are disturbances in the fabric of spacetime caused by movements of masses in the universe. Predicted by Albert Einstein in 1916 as a consequence of his General Theory of Relativity, gravitational waves carry information about their origins as well as about the nature of gravity itself, providing insights into regions of the cosmos that are otherwise hidden from view. In particular, they may be helpful to:

- Detect astrophysical events or entities that due to their physical nature are impossible to detect in the electromagnetic signatures, such as the case of black holes and their dynamics;
- Reveal information about the internal structure of astrophysics bodies such as neutron stars and events such as supernovae. Indeed, traveling unimpeded through internal layers, they provide unique insight into physics below the surface level of an event.

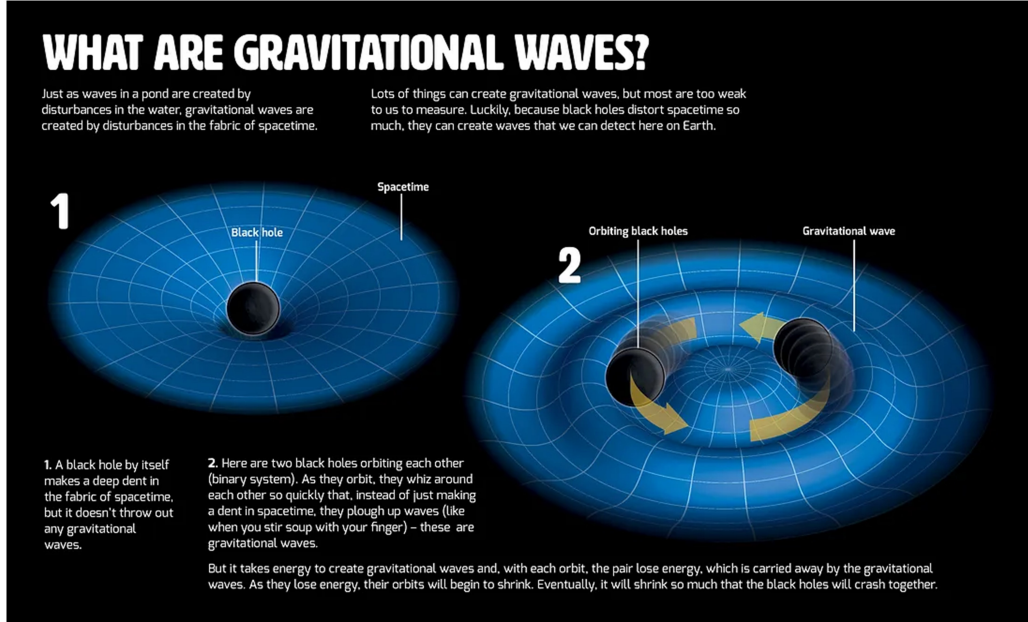


Figure 1. Illustration of the underlying physics of gravitational waves.

Figure 2. Visual Guide to Gravitational Waves.

- Correlate distinct astronomical phenomena, with particular relevance to explain intense and localized phenomena in the electromagnetic spectrum (e.g. gamma-ray bursts and merging of binary neutron stars).

The innerworkings of gravitational waves stem directly from Einstein's field equations of general relativity(GR), which describe how matter and energy influence the curvature of spacetime¹. In very generic terms, GR does not allow the instantaneous (which would violate causality) Newton-gravity interaction but instead introduces a formalism where massive objects distort spacetime which in turn influences the dynamics of bodies. Besides, as this distortion is not instantaneous, it propagates outward at the speed of light in the form of *gravitational waves* when the mass undergoes acceleration, particularly asymmetric acceleration such as in binary orbits. Adding to solving the causality, GR explains also gravitational redshifts, gravitational lensing, and the anomalous precession of the orbit of Mercury around the Sun, being one of the most successful physical theories of the 20th century. A complete derivation of the formalism to describe gravitational waves would require an entire course of GR which is not the intent of this chapter². But we can start by introducing the Einstein equation as the foundation of general relativity, describing how matter and energy influence the curvature of spacetime as

$$G_{\mu\nu} + \Lambda g_{\mu\nu} = \frac{8\pi G}{c^4} T_{\mu\nu} \quad (1.1)$$

¹ Matter tells spacetime how to curve, and spacetime tells matter how to move. - John Wheeler

² A good reference to start such endeavor would be "A first course in general relativity" by Schultz

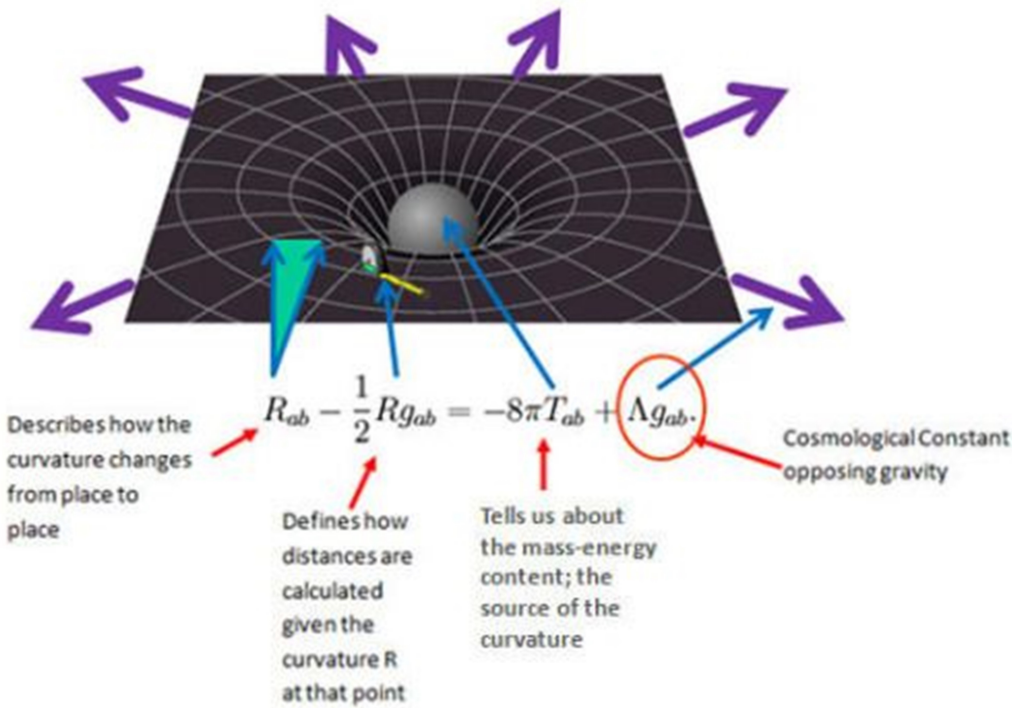


Figure 3. Illustration of the underlying physics of Einstein Equation

with $G_{\mu\nu}$ the Einstein tensor, Λ the cosmological constant, $g_{\mu\nu}$ the metric tensor, G the gravitational constant, c the speed of light and $T_{\mu\nu}$ the stress-energy tensor. In short, the Einstein tensor can be constructed mathematically from the metric as

$$G_{\mu\nu} = R_{\mu\nu} - \frac{1}{2}g_{\mu\nu}R \quad (1.2)$$

where the scalar curvature R is the trace of the Ricci tensor $R_{\mu\nu}$, i.e.

$$R = g^{\mu\nu}R_{\mu\nu} \quad (1.3)$$

which in turn is obtained from the Riemann tensor as

$$R_{\mu\nu} = R_{\mu\lambda\nu}^\lambda. \quad (1.4)$$

The Riemann curvature tensor is obtained from

$$R_{\sigma\mu\nu}^\rho = \partial_\mu\Gamma_{\nu\sigma}^\rho - \partial_\nu\Gamma_{\mu\sigma}^\rho + \Gamma_{\mu\lambda}^\rho\Gamma_{\nu\sigma}^\lambda - \Gamma_{\nu\lambda}^\rho\Gamma_{\mu\sigma}^\lambda \quad (1.5)$$

where the Christoffel symbols of the second kind are given by

$$\Gamma_{\mu\nu}^\rho = \frac{1}{2}g^{\rho\sigma}(\partial_\mu g_{\sigma\nu} + \partial_\nu g_{\sigma\mu} - \partial_\sigma g_{\mu\nu}) \quad (1.6)$$

On its side, the energy-momentum tensor represents the distribution and

Figure 4. Polarization of gravitational waves.

flow of energy and momentum in spacetime, with derivation depending on the context. But overall, the Einstein equation relates how matter and energy influence the metric of spacetime, affecting the equations of motion of matter in this way. Straightforwardly, any changes of matter and energy propagate as a perturbation of the metric as **gravitational waves**.

For simplicity, we usually assume that the spacetime is only slightly perturbed from a flat condition. In such a case, the metric tensor, which describes spacetime curvature, can be expressed as

$$g_{\mu\nu} = \eta_{\mu\nu} + h_{\mu\nu} \quad (1.7)$$

where $\eta_{\mu\nu}$ represents the Minkowski (flat spacetime) metric and $h_{\mu\nu}$ represents a small perturbation due to gravitational waves. Using the linearized version of Einstein's equations under the assumption of weak fields, and for a particular gauge choice, the wave equation for the perturbations can be derived as

$$\left(\nabla^2 - \frac{1}{c^2} \partial_{t^2}\right) h_{\mu\nu} = -\frac{16\pi G}{c^4} T_{\mu\nu} \quad (1.8)$$

which can be simplified in vacuum using $T_{\mu\nu} = 0$. A common choice for $h_{\mu\nu}$ in this case is to warrant that it is transverse and traceless, meaning that for a wave propagating in the z direction, it can be written as

$$h_{\mu\nu} = \begin{pmatrix} 0 & 0 & 0 & 0 \\ 0 & h_+ & h_\times & 0 \\ 0 & h_\times & -h_+ & 0 \\ 0 & 0 & 0 & 0 \end{pmatrix} \quad (1.9)$$

where h_+ and h_\times can be understood as the amplitudes of the gravitational waves in two orthogonal polarizations (plus and cross), that will depend on the orientation of the source dynamics relative to the detector but that:

- Plus: stretches and compresses space along the x and y axes, respectively;
- Cross: stretches and compresses space but at 45-degree angles to the plus polarization.

In this picture, gravitational waves traveling through Earth cause tiny oscillations in spacetime, alternately stretching and compressing distances but by an amount so small that detecting them is a significant technological challenge. As an influence in the metric, gravitational waves produce a **strain** in

Figure 5. The ecosystem of GW detection in terms of frequency.

spacetime, meaning that its effect will only be felt when measuring the distance between two points in space. Roughly speaking, if completely oriented with the polarization of the wave, the deformation from the initial distance L will be equal to

$$\Delta L = |h_{\mu\nu}|L \quad (1.10)$$

1.1 How intense are these?

The gravitational wave equation does not seem friendly itself and in practice is extremely hard to tackle in an analytical manner. A popular method is to utilize a multipolar expansion, which leads to a quadrupole moment contribution that can be used to derive some figures of merit for the case of two-point masses in circular orbit about a common center of mass and that describes the binary merger of neutron stars and black holes, two of the most intense gravitational phenomena in the universe³.

Using some approximations that we will not describe in detail but that can be found elsewhere⁴ it is possible to put a number in the fluctuations in spacetime on the order of

$$|h_{\mu\nu}| \approx 10^{-21} \quad (1.11)$$

and frequencies up to

$$f_{gw} \approx 800 Hz. \quad (1.12)$$

meaning that ultimately we need to measure minuscule strains at audio frequencies, where environmental noise is abundant.

³ and thus, the more likely to be "observed" in LIGO

⁴ e.g. "Squeezed Vacuum Injection in Advanced LIGO: Enhancing Gravitational-Wave Detection Using Quantum States of Light" by Maggie Tse

2 LIGO: The Classical Design

The Laser Interferometer Gravitational-Wave Observatory (LIGO) was conceived with the goal of directly detecting gravitational waves. It employs optical interferometric concepts and is perhaps the most famous and versatile type of gravitational wave detector (others are Pulsar Timing Arrays - measuring the time variations of pulsar systems - and the future LISA, a space-based interferometer). The conceptual groundwork for LIGO began in earnest in the 1970s, led by pioneers like Rainer Weiss, Kip Thorne, and Ronald Drever, who proposed using laser interferometry to detect gravitational waves. The principle behind the detection method involves measuring the minute changes in distance between two test masses positioned kilometers apart, changes expected to be induced by a passing gravitational wave.

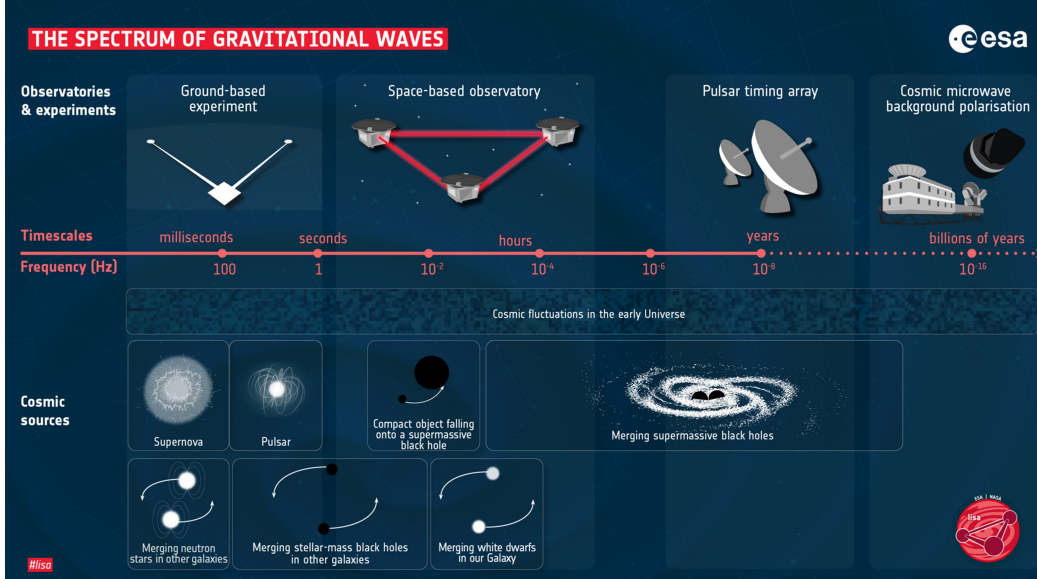


Figure 6. Timescales of gravitational waves from distinct cosmological events.

In 1992, the National Science Foundation (NSF) approved funding for LIGO construction, and by 2002, the observatories at Hanford, Washington, and Livingston, Louisiana, were operational. The first direct detection of gravitational waves by LIGO in September 2015 marked a seminal moment in physics and astronomy. This detection (event GW150914) was sourced to the merger of two black holes approximately 1.3 billion light-years away and confirmed the robustness of general relativity in the strong-field regime. Since then, LIGO, in conjunction with Virgo and other observatories, has detected several more gravitational wave events, each adding to our understanding of the universe.

2.1 The Overall Design and Notes on Components

At its heart, LIGO employs a Michelson interferometer, a design that we already discussed and that has multiple connections with astronomy and cosmology in different epochs of time. The design is simple in concept but extraordinarily complex in execution at LIGO. It consists of two perpendicular arms, each extending four kilometers in length, within which laser light is split into two beams that travel back and forth along the arms. In particular, let us introduce some notes on its components:

Laser: The primary light source in LIGO is a neodymium-doped yttrium aluminum garnet (Nd:YAG) laser capable of emitting a highly stable and coherent beam of light at 1064 nanometers. This laser type is chosen for its high power stability and minimal phase noise, crucial for the precise

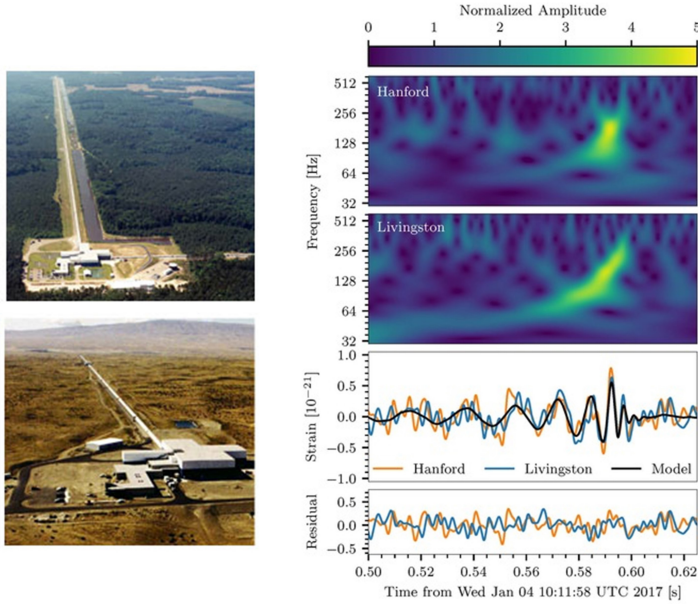


Figure 7. LIGO facilities in Washington and Livingstone and first event detection in 2015.

measurements required in gravitational wave detection. Typically, the laser output in LIGO operates at a power of about 200 watts.

Test Masses and Mirrors: At the heart of LIGO's detection capability are its test masses—four ultra-precise mirrors, two at each site, which serve as the endpoints of the interferometer's arms. These mirrors are made from fused silica, chosen for its low thermal expansion properties and excellent optical quality. Each mirror is meticulously polished to achieve the required flatness and is coated with multiple layers of reflective material to maximize the reflection of laser light. The mirrors also function as test masses due to their substantial mass (about 40 kilograms), helping to isolate them from external vibrations and noise.

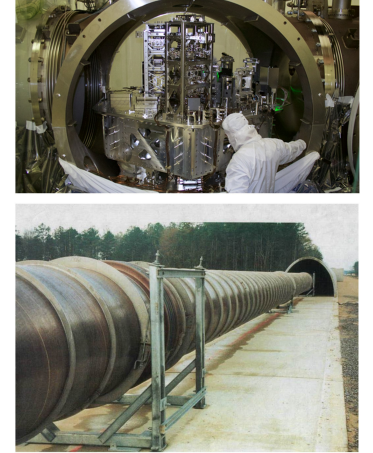
Vacuum System; LIGO's optical components are housed within an immense vacuum chamber, one of the largest and most pristine in the world, boasting a volume of 10,000 cubic meters (353,000 cubic feet) and maintaining a pressure of 10^{-9} Torr, or one-trillionth of an atmospheric pressure. This level of vacuum is surpassed only by that of the Large Hadron Collider in Switzerland. The primary purpose of such an extreme vacuum is to eliminate air molecules and microscopic debris, preventing them from i)affecting measurements and ii)settling on LIGO's mirrors or other optical elements. If contaminants were to come into contact with



Figure 8. Mirrors of LIGO.

the laser beam, they could vaporize and potentially cause irreparable damage to the equipment (each test-mass mirror is valued at approximately 2 million dollars).

Achieving the requisite vacuum conditions within LIGO's chambers involved a lengthy process: it took 1,100 hours (about 40 days) of continuous pumping to reach the optimal operational pressure. During this phase, turbo-pump (jet) vacuums initially removed the majority of the air. Concurrently, the vacuum tubes were heated to temperatures between 150-170 degrees Celsius for 30 days to eliminate any residual gases and moisture embedded in the steel, ensuring the integrity and functionality of the vacuum environment.



2.2 Michelson Interferometer and Dark fringe Operation

In LIGO, the Michelson interferometer is used to measure the difference in path length between its two arms. When a gravitational wave passes through the interferometer, it changes the relative length of the arms very slightly due to the stretching and squeezing of spacetime, which alters the interference pattern observed at the detector due to the introduction of a phase difference. As we saw in previous weeks, the output at the anti-symmetric port for a Michelson will be given

$$I_{PD} = \frac{I_0}{2}(1 + \cos(2\Delta\phi + \phi_0)) \quad (2.1)$$

where ϕ_0 encloses the initial condition for operation whereas $\Delta\phi$ corresponds to the difference in the optical path due to the strain in the spacetime. When completely aligned with the polarization of the gravitational wave we have

$$\Delta\phi = \frac{2\pi h(t)L}{\lambda} \quad (2.2)$$

valid for time-varying strain $h(t)$ with a period much longer than the total round-trip of light in each arm.

In LIGO, and contrary to the cases we previously described in the last weeks, the point of operation is close to the **Dark Fringe** instead of the quadrature point.

Indeed, this point comes with non-trivial advantages:

- **Sensitivity to noise:** while at the quadrature point the sensitivity to changes is maximized, the sensitivity to noise is also maximum.
- **Visibility:** operating near the dark fringe, LIGO ensures that the baseline signal is minimal, thereby maximizing the contrast and visibility of

Figure 9. Every part of LIGO is in a vacuum - even the 4km arms.

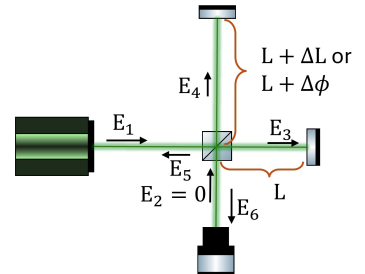


Figure 10. Simplified Scheme of the LIGO Michelson interferometer

any signals produced by gravitational waves.

- **Controllability:** Operating near the dark fringe provides a stable and well-defined reference point for calibration and control systems. It simplifies the process of adjusting the interferometer's settings to maintain optimal sensitivity and ensures that the system's response to gravitational waves can be accurately modeled and predicted. The control systems can maintain the operational point with greater precision when starting from a state of minimal light intensity, where deviations are more easily detectable and correctable.

In dark fringe operation, the interferometer is tuned such that in the absence of a gravitational wave, the path length difference causes the beams to recombine destructively, resulting in minimal or no light intensity at the detector (a dark fringe). Experimentally we choose $\phi_0 = (2m + 1)\pi$ with m an integer corresponding to a case where (utilizing $\lambda = 2\pi c/\omega$) the power at the detector is given by

$$P_{PD} = P \sin^2 \left(2\pi \frac{\Delta L}{\lambda} \right) \approx P \frac{4\omega^2}{c^2} (\Delta L)^2 \quad (2.3)$$

with P being the laser power entering the interferometer.

2.3 Fabry-Perot

The arms of LIGO are approximately 4km long, meaning that the total length change for the numbers introduced before is around

$$\Delta L \approx |h|L \approx 10^{-18} m \quad (2.4)$$

which is still 1000 times smaller than the size of the proton. One can substitute directly into the expression for the power of the photodetector and obtain an extremely small value of $P_{PD} \approx 10^{-22} W$. Taking into consideration that the energy for a single photon at 1064nm is around $1.8 \times 10^{-19} J$ this means that we will be looking at a single photon arriving at each 3 minutes. In practice, this means that while 4-km-long arms already seem enormous, they would still be too short to enable the detection of gravitational waves. Indeed, a good target to warrant detection will be above the femtowatt range (around thousands of photons per second, around 10 per millisecond, allowing to reach the 1000Hz frequency range).

A way to provide additional path length is to alter the Michelson interferometer to include Fabry-Perot cavities, just like in the Fabry-Perot interferometer we described in previous weeks. In this case, an additional mirror is placed in each arm near the beamsplitter and 4 km from the mirror at the end

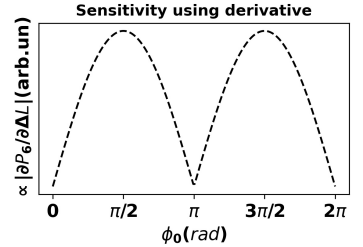


Figure 11. In LIGO the operation point is the dark fringe $\phi_0 = (2m + 1)\pi$ and not the quadrature point $\phi_0 = (2m + 1)\pi/2$.

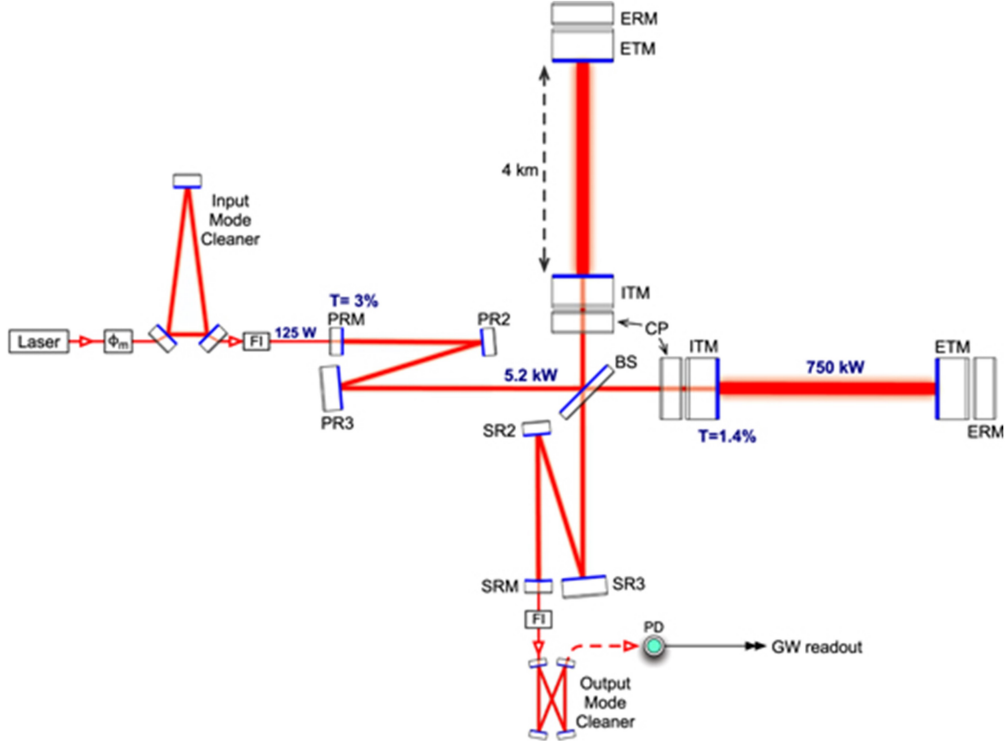


Figure 12. Closer to LIGO actual setup, adding a Fabry-Perot (ITM-ETM) in each path to increase effective path distance, together with the power recycling mirrors (PR).

of that arm. In practice, after entering the instrument via the beam splitter, it can be shown that a Fabry-Perot cavity in such configuration would lead to an increase of the effective path length from L to

$$L_{eff} = \mathcal{F}/\pi \quad (2.5)$$

where \mathcal{F} is the Finesse of the Fabry-Perot cavity.

In the existing configuration $\mathcal{F} \approx 300$ which increases the effective distance traveled by each laser from 4 km to about 1200 km, increasing the signal at the photodetector by two orders of magnitude. Still, it is not yet sufficient to reach the femtowatt or above level we previously introduced as a ballpark figure for gravitational wave detection.

2.4 Power Recycling

Looking at the expression of the power reaching the photodetector one can see that another strategy to increase the signal is to increase the power of the laser itself. While this is somehow difficult to do on the side of the laser itself, the operation in the dark fringe mode allows to employ power recycling strategies, increasing the effective power of the laser light within the

interferometer without increasing the actual laser output. This is achieved through the use of a power recycling mirror placed strategically in the LIGO setup.

The power recycling mirror (PRM) is located at the symmetric port of the interferometer (the port of the laser) and in short it exploits the fact that most of the power exits the interferometer from the original input port. Assuring that:

- the mirror is positioned in such a way that it contributes constructively to the input of the laser;
- the transmissivity of the PRM matches the level of optical loss inside the Michelson, optimizing the coupling of light into the Michelson in the form of impedance matching between the input and the interferometer

allows to utilize the optical power that does not dissipate nor exit the interferometer from the anti-symmetric port to be recirculated rather than re-entering the laser. Indeed, it is possible to demonstrate that this boost corresponds to an effective laser power of approximately 750kW, meaning that a signal in the range of $10^{-15}W - 10^{-13}W$ will be available for detection at the anti-symmetric port.

3 The Noise Limitations

At this point, and classically, we are ready to detect gravitational waves with this LIGO system. Yet, being such small variations, understanding and mitigating noise - in particular in the expected frequency bands - is of fundamental importance. We can divide the noise into two large families: **displacement noise** and the **phase noise**.

Displacement noise: Displacement noise is associated with the unwanted motion of test masses. Dividing in the major sources we have:

- **Ground vibration (including seismic):** occurring at low frequencies (below 1Hz) and can be mitigated by a combination of passive isolation through pendulum systems and active feedback control. Besides, being geographically isolated also contributes to lowering this noise.
- **Thermal noise:** coming from the optical elements - mostly from the optical coatings than from the fused silica itself - and the suspensions of the test masses - fused silica fibers that hang the test masses. The thermal noise contribution is typically small, but future state-of-the-art research is set to target these limits with research

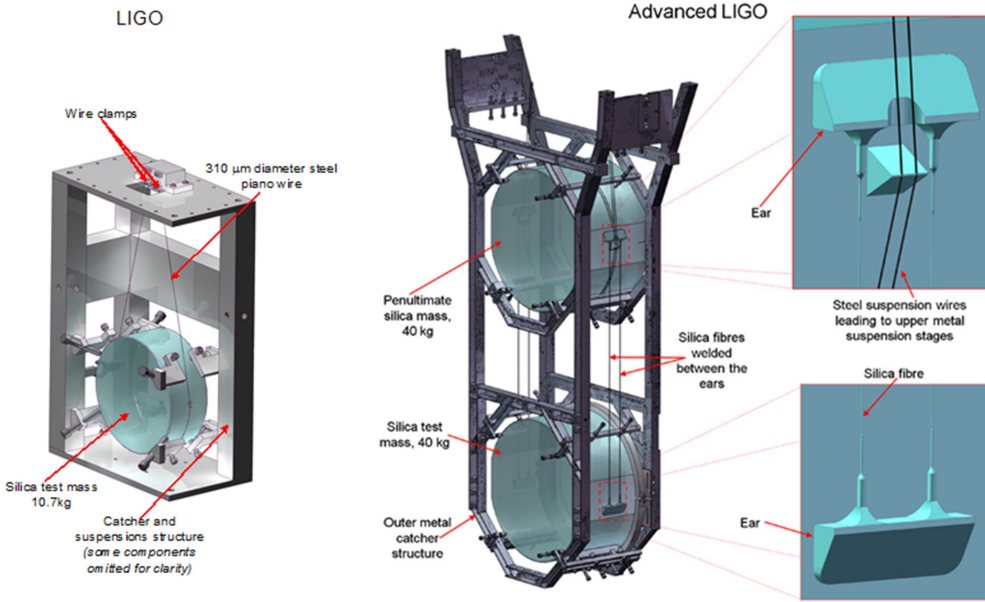


Figure 13. Mitigating ground vibration via freely moving mirrors suspended by thin fibers and differences between LIGO and Advanced LIGO configurations. Starting in 2010, the major reduction in noise of the Advanced LIGO redesign allowed us to observe in 2015 the first event.

into new materials and the choice of geometry for the suspension fibers.

Phase noise: Associates to the unwanted phase shifts and its primary sources are:

- **Residual gas:** small contribution due to the presence of residual atoms in the beam path, but very small due to the vacuum configuration;
- **Scattered light:** arises from imperfections in optics, which can scatter light out of the main beam. This light can then acquire phase shifts by reflecting off vibrating components such as the beam tube and other hardware inside the vacuum chambers, before recombining with the main beam and reaching the readout. Typically dominates below 50Hz.
- **Quantum Fluctuations:** statistical fluctuations in photon arrival times at the readout which can be interpreted as phase fluctuations.

Thus being said, engineering advances play an important role in reducing the noise in LIGO, allowing to mitigate most in classical manners. Yet, the

quantum noise represents a fundamental barrier that even if all the other sources of noise are mitigated in classical manners, there would still be a noise level at the detection - the **quantum noise limit**.

3.1 The Quantum Noise Limit

To understand where the quantum noise terms come from we will need to delve deeper into the fundamental physics of the electromagnetic field. From a quantum perspective, we know that photons are in practice discrete quanta of energy that can be measured by photodetectors. This means that there is an intrinsic **discretization** which ultimately may lead to two distinct effects:

- **Shot noise:** arises from statistical fluctuations in the arrival time of photons at the interferometer output, which can resemble a phase shift.
- **Radiation pressure noise:** with such large effective powers, light in each cavity transfers a non-negligible amount of momentum to the suspended mirrors. Even with the 40 kg mirrors, quantum fluctuations in the field amplitude will translate into fluctuations in the mirror momentum. Varying the mirror position will alter the interferometric conditions and the phase of the light, manifesting as a quantum radiation pressure noise at the exit photodetector.

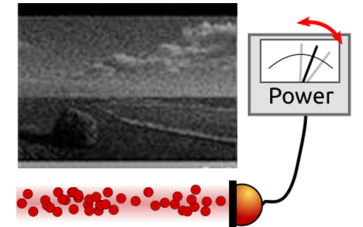


Figure 14. Fluctuations on the arrival time of photons lead to shot noise. This is also observed in low lighting photography.

Before we advance, we should note that quantum noise is not a single number but a continuous, random function of time whose strength varies dramatically with frequency. Taking into consideration the precision required by LIGO, the displacement signal ΔL can be considered as a stationary stochastic process and ask how much variance lives at each Fourier frequency. This recovers the definition of the power spectral density

$$S_{xx}(f) = \lim_{T \rightarrow \infty} \frac{1}{T} |\hat{x}_T(f)|^2 \quad (3.1)$$

with $\hat{x}_T(f)$ being the Fourier transform of signal x , which relates with the uncertainty per unit bandwidth around f as

$$u_{\Delta L}(f) = \sqrt{\text{Var}(x)} = \sqrt{S_{xx}(f)}. \quad (3.2)$$

3.2 Shot Noise Contribution

Shot noise is a quantum-measurement noise associated with the discrete nature of photons arriving on the detection photodiode. Considering the sim-

plest Michelson interferometer we have

$$P_{PD} = P \sin^2 \left(2\pi \frac{\Delta L}{\lambda} \right) \approx P \frac{\omega^2}{c^2} (\Delta L)^2 \quad (3.3)$$

for which the one-sided spectral density of the power is given by

$$S_{PD}^{SN} = 2\hbar\omega P_{PD}. \quad (3.4)$$

To transform this to the noise in ΔL measurement we can utilize the fact that for small ΔL we may expand obtain $P_{PD} \approx (\partial P_{PD}/\partial \Delta L)\Delta L$ or in the converse form $\Delta L \approx P_{PD}(\partial P_{PD}/\partial \Delta L)^{-1}$ to obtain

$$S_{\Delta L}^{SN} = \frac{2\hbar\omega P_{PD}}{(\partial P/\partial \Delta L)^2} = \frac{2\hbar\omega P_{PD}}{4\omega^2/c^2 P P_{PD}} = \frac{\hbar c^2}{2\omega P} \quad (3.5)$$

Finally one can get the shot noise limited length difference noise from the square root of this power:

$$u_{\Delta L}^{SN} = \sqrt{S_{\Delta L}^{SN}} = c \sqrt{\frac{\hbar}{2\omega P}} \quad (3.6)$$

which is given in units of $m\sqrt{Hz}^{-1}$ ⁵. From this formula, we can right away conclude a few things:

- The shot noise is independent of the frequency of the oscillating strain, being thus of the white noise type;
- The shot noise is independent of the power reaching the photodetector;
- The shot noise can be reduced by increasing the power inside the interferometer.

⁵ In practice, this gives the error in the frequency space, which is convenient for this case.

Thus, we can conclude that operating near a dark fringe with a low output power is indeed the ideal condition to reduce shot noise.

Note that in the case of the Michelson interferometer with the additional Fabry-Perot in each arm, there is an additional multiplicative term in the shot noise as

$$u_{\Delta L}^{SN,FP} = u^{SN} (1 + i2\Omega\tau_s) \quad (3.7)$$

where τ_s corresponds to the storage time of the arm cavities. This adds a dependency on the gravitational wave frequency that for the sake of simplicity we will ignore in the following sections.

3.3 Radiation Pressure Noise

Radiation pressure noise in LIGO results from the momentum transfer of photons to the mirrors. As photons reflect off the mirrors, they exert a force due to their momentum, causing tiny fluctuations in the position of the mirrors. These fluctuations contribute to noise in the measurement of gravitational waves, particularly at lower frequencies.

The mirror can be modeled as a harmonic oscillator of angular frequency Ω_0 and mass m with the equation of motion given by

$$m\ddot{x} + m\Omega_0^2 x = F \quad (3.8)$$

which solved in the Fourier space assuming the free mass regime $\Omega_0 \ll \Omega$, being Ω the angular frequency of the GW wave, leads to

$$\hat{x}(\Omega) = \frac{2P}{m\Omega^2 c} \quad (3.9)$$

where we substituted the force $F = 2P/c$ for the photons reaching the mirror. The power spectral density for x and consequently ΔL can be obtained from the definition and the spectral density for the power $S_P = 2\hbar\omega P$, obtaining the differential arm length due to radiation pressure noise is then given by

$$S_{\Delta L}^{RPN} = \frac{8\hbar\omega P}{m^2\Omega^4 c^2} \quad (3.10)$$

which is associated to a limit

$$u_{\Delta L}^{RPN} = \sqrt{S_{\Delta L}^{RPN}} = \frac{2}{m\Omega^2 c} \sqrt{2\hbar\omega P}. \quad (3.11)$$

Analyzing the equation, we see that:

- the noise is frequency dependent, and decreases with frequency;
- increasing the circulating power adds more noise, but increasing the mirror masses can be used to arbitrarily reduce the impact of quantum noise.

3.4 Reducing noise classically

From the noise derived in the previous sections, it appears that one can increase the circulating power in the interferometer arbitrarily to reduce shot noise, while simultaneously increasing the mirror mass to compensate for the power increase, and thus still reduce radiation pressure noise. However, in practice, this would lead to encountering other limits for the usual behavior. First, the thermal deformation of the mirrors due to light absorption

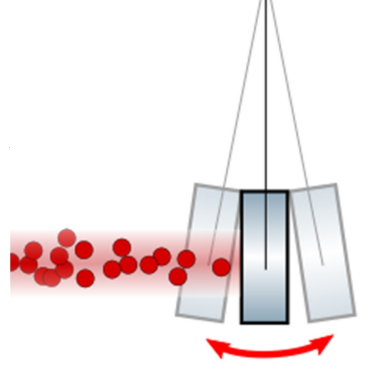


Figure 15. Fluctuations on the arrival time of photons in the mirrors may also lead to radiation pressure noise.

each photon carries $p = h/\lambda = \hbar\omega/c$ and is reflected

would create thermal lensing, requiring further compensation. Then, the mirror mass is limited by the ability to produce large polished mirrors, and the ability to suspend them. In this case, solving quantum problems with classical techniques can only get us so far, once we reach the limits of current technology.

4 Quantum Limit and Beyond

From the equations introduced before it is possible to compute a lower boundary for the sum $u_{\Delta L}^{SN} + u_{\Delta L}^{RPN}$ by carefully choosing P and assuming **no correlations between shot noise and radiation pressure noise**. Indeed, by computing the minimum in relation to P and substituting this value, it is straightforward to obtain the minimum

$$u_{\Delta L}^{SQL} = \sqrt{S_{\Delta L}^{SQL}(\Omega)} = \frac{1}{\Omega} \sqrt{\frac{2\hbar}{m}} \quad (4.1)$$

which is denoted the **standard quantum limit**, represented Figure 16. In essence, the SQL is a manifestation of the Heisenberg uncertainty principle, and represents the best quantum noise performance achievable in an interferometer without the use of nonclassical techniques. In practice, from the perspective of gravitational-wave astrophysics, this limits the higher measurement precision in an interferometer and the detection of fainter signals from smaller and more distant objects. So, can we go beyond it?

4.1 The origin of the noise

To really understand where the noise comes from, we will need to enter into a full quantum picture. We will not enter into detail on the quantum theory itself and try to get only the necessary tools along the way. Yet keep in mind that the end goal is to understand two key concepts: the ground state fluctuations of the electromagnetic field, and what happens in a quantum version of a beamsplitter.

4.1.1 Quantization of the Electromagnetic Field

First, we will start with the quantization of the electromagnetic field. This process involves promoting the classical electromagnetic fields to quantum operators and expressing them in terms of creation and annihilation operators, and starts from the vector potential.

The classical electromagnetic field can be described by the vector potential $\mathbf{A}(\mathbf{r}, t)$ and the scalar potential $\phi(\mathbf{r}, t)$. The electric and magnetic fields are

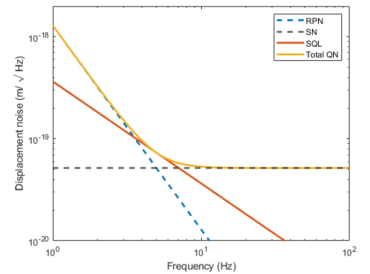


Figure 16. Shot Noise, Radiation Pressure, and Standard Quantum Limit, computed for a displacement noise spectral density for a Michelson interferometer with mirrors 10kgs mass suspended as pendulums and a total light power of 1MW.

given by:

$$\mathbf{E}(\mathbf{r}, t) = -\nabla\phi - \frac{\partial\mathbf{A}(\mathbf{r}, t)}{\partial t},$$

$$\mathbf{B}(\mathbf{r}, t) = \nabla \times \mathbf{A}(\mathbf{r}, t).$$

By choosing the Coulomb gauge, where $\nabla \cdot \mathbf{A} = 0$, we can describe the vector potential in terms of two orthogonal transverse vectors (corresponding to polarizations). The vector potential $\mathbf{A}(\mathbf{r}, t)$ can be expanded as a sum over modes characterized by the wave vector \mathbf{k} and polarization index λ :

$$\mathbf{A}(\mathbf{r}, t) = \sum_{\mathbf{k}, \lambda} \left(\mathcal{A}_{\mathbf{k}, \lambda} \mathbf{e}_{\mathbf{k}, \lambda} e^{i(\mathbf{k} \cdot \mathbf{r} - \omega_{\mathbf{k}} t)} + \mathcal{A}_{\mathbf{k}, \lambda}^* \mathbf{e}_{\mathbf{k}, \lambda}^* e^{-i(\mathbf{k} \cdot \mathbf{r} - \omega_{\mathbf{k}} t)} \right),$$

where $\mathcal{A}_{\mathbf{k}, \lambda}$ are the complex amplitudes of the vector potential, $\mathbf{e}_{\mathbf{k}, \lambda}$ are the polarization vectors, and $\omega_{\mathbf{k}} = c|\mathbf{k}|$ is the angular frequency of the mode.

Now, to quantize the electromagnetic field, we simply promote the classical field amplitudes to quantum operators. The vector potential is then expressed in terms of the creation and annihilation operators $\hat{a}_{\mathbf{k}, \lambda}$ and $\hat{a}_{\mathbf{k}, \lambda}^\dagger$:

$$\hat{\mathbf{A}}(\mathbf{r}, t) = \sum_{\mathbf{k}, \lambda} \sqrt{\frac{\hbar}{2\epsilon_0\omega_{\mathbf{k}}V}} \left(\hat{a}_{\mathbf{k}, \lambda} \mathbf{e}_{\mathbf{k}, \lambda} e^{i(\mathbf{k} \cdot \mathbf{r} - \omega_{\mathbf{k}} t)} + \hat{a}_{\mathbf{k}, \lambda}^\dagger \mathbf{e}_{\mathbf{k}, \lambda}^* e^{-i(\mathbf{k} \cdot \mathbf{r} - \omega_{\mathbf{k}} t)} \right),$$

where $\hat{a}_{\mathbf{k}, \lambda}$ and $\hat{a}_{\mathbf{k}, \lambda}^\dagger$ are the annihilation and creation operators for the mode (\mathbf{k}, λ) , V is the quantization volume, and ϵ_0 is the permittivity of free space.

Assuming vacuum, i.e. $\phi = 0$, and using the quantized vector potential, the electric and magnetic fields can be written as:

$$\hat{\mathbf{E}}(\mathbf{r}, t) = i \sum_{\mathbf{k}, \lambda} \sqrt{\frac{\hbar\omega_{\mathbf{k}}}{2\epsilon_0 V}} \left(\hat{a}_{\mathbf{k}, \lambda} e^{i(\mathbf{k} \cdot \mathbf{r} - \omega_{\mathbf{k}} t)} - \hat{a}_{\mathbf{k}, \lambda}^\dagger e^{-i(\mathbf{k} \cdot \mathbf{r} - \omega_{\mathbf{k}} t)} \right) \mathbf{e}_{\mathbf{k}, \lambda},$$

$$\hat{\mathbf{B}}(\mathbf{r}, t) = \sum_{\mathbf{k}, \lambda} \sqrt{\frac{\hbar\omega_{\mathbf{k}}}{2\mu_0 V}} \left(\hat{a}_{\mathbf{k}, \lambda} e^{i(\mathbf{k} \cdot \mathbf{r} - \omega_{\mathbf{k}} t)} + \hat{a}_{\mathbf{k}, \lambda}^\dagger e^{-i(\mathbf{k} \cdot \mathbf{r} - \omega_{\mathbf{k}} t)} \right) (\hat{\mathbf{k}} \times \mathbf{e}_{\mathbf{k}, \lambda}),$$

where μ_0 is the permeability of free space.

Finally, the Hamiltonian of the quantized electromagnetic field can be derived from the energy density of the electric and magnetic fields. It is given by:

$$\hat{H} = \frac{1}{2} \int \left(\epsilon_0 |\hat{\mathbf{E}}(\mathbf{r}, t)|^2 + \frac{1}{\mu_0} |\hat{\mathbf{B}}(\mathbf{r}, t)|^2 \right) d^3 r.$$

Substituting the expressions for $\mathbf{E}(\mathbf{r}, t)$ and $\mathbf{B}(\mathbf{r}, t)$, and integrating over the volume, we obtain:

$$\hat{H} = \sum_{\mathbf{k}, \lambda} \hbar\omega_{\mathbf{k}} \left(\hat{a}_{\mathbf{k}, \lambda}^\dagger \hat{a}_{\mathbf{k}, \lambda} + \frac{1}{2} \right).$$

This is the Hamiltonian in terms of the creation and annihilation operators, showing the quantized nature of the electromagnetic field.

4.1.2 States and Operators to handle the quantized electromagnetic field

In practice, after the quantization of the electromagnetic field, we end up working in terms of states and operators. There will be two types of states - the Fock states and Coherent states - which are closely related to the action of the creation and annihilation operators.

Properties of the Creation and Annihilation operators: As introduced in the quantization step, the Creation and Annihilation operators feature very interesting properties that we must first introduce.

Action on Fock States: These operators are defined by their action on the Fock basis (or number basis), given by

$$\hat{a}|n\rangle = \sqrt{n}|n-1\rangle, \quad (4.2)$$

and

$$\hat{a}^\dagger|n\rangle = \sqrt{n+1}|n+1\rangle. \quad (4.3)$$

Canonical commutation relations: The creation and annihilation operators satisfy the following canonical commutation relations:

$$[\hat{a}, \hat{a}^\dagger] = 1, \quad (4.4)$$

and

$$[\hat{a}, \hat{a}] = [\hat{a}^\dagger, \hat{a}^\dagger] = 0. \quad (4.5)$$

Vacuum State: In the Fock basis the vacuum state is given by $|0\rangle$ and is annihilated by \hat{a}

$$\hat{a}|0\rangle = 0 \quad (4.6)$$

while \hat{a}^\dagger generates the first excited state

$$\hat{a}^\dagger|0\rangle = |1\rangle. \quad (4.7)$$

Number Operator: The number operator is just

$$\hat{n} = \hat{a}^\dagger\hat{a}. \quad (4.8)$$

and it gives the number of photons in the state

$$\hat{n}|n\rangle = n|n\rangle. \quad (4.9)$$

Beamsplitters and interferometers: To handle the same matrix formalism of the classical field applies, e.g. for a beamsplitter

$$\begin{bmatrix} \hat{a}_3 \\ \hat{a}_4 \end{bmatrix} = \overline{BS} \begin{bmatrix} \hat{a}_1 \\ \hat{a}_2 \end{bmatrix} \quad (4.10)$$

which is very convenient to keep track of all the contributions of the fields at the output ports.

Hamiltonian: Using these operators, it is possible to write the Hamiltonian for the electromagnetic field as

$$\hat{H} = \hbar\omega \left(\hat{a}^\dagger \hat{a} + \frac{1}{2} \right). \quad (4.11)$$

which means that the vacuum state has an energy contribution!

Exercise 1. Using the action of the operators on the Fock basis, demonstrate the commutation relations.

In addition to the Fock states (or number states), coherent states are particularly relevant when handling real experimental conditions. Indeed, these approximate quite well the output of a laser beam.

Coherent states: these states are particularly important in the context of quantum optics as they can be used to describe laser light. A coherent state $|\alpha\rangle$ may be constructed in the Fock basis as

$$|\alpha\rangle = \exp\left(\frac{-|\alpha|^2}{2}\right) \sum_{n=0}^{\infty} \frac{\alpha^n}{\sqrt{n!}} |n\rangle \quad (4.12)$$

and it can be demonstrated that it is an eigenstate of the annihilation operator

$$\hat{a}|\alpha\rangle = \alpha|\alpha\rangle, \quad (4.13)$$

and can be constructed from the vacuum state by applying the displacement operator

$$|\alpha\rangle = D(\alpha)|0\rangle, \quad (4.14)$$

given by

$$D(\alpha) = \exp\left(\alpha\hat{a}^\dagger - \alpha^*\hat{a}\right). \quad (4.15)$$

Note that for such a state, both the mean number of photons $\langle\alpha|\hat{n}|\alpha\rangle$ and variance $\langle\alpha|\hat{n}^2|\alpha\rangle - \langle\alpha|\hat{n}|\alpha\rangle^2$ equals to $|\alpha|^2$.

Another interesting fact is that the probability of finding a state of n

photons in the coherent state follows a Poisson distribution given by

$$P(n) = |\langle n | \alpha \rangle|^2 = \frac{|\alpha|^{2n} e^{-|\alpha|^2}}{n!} \quad (4.16)$$

Exercise 2. Demonstrate that the coherent state is an eigenstate of the annihilation operator.

Exercise 3. Demonstrate that the $P(n) = |\langle n | \alpha \rangle|^2 = \frac{|\alpha|^{2n} e^{-|\alpha|^2}}{n!}$.

Finally, a very interesting tool to deal with some calculations that will follow are the quadrature operators.

Quadrature operators: The quadrature operators are two operators that can be defined in terms of the creation and annihilation operators as

$$\hat{X} = \frac{\hat{a} + \hat{a}^\dagger}{2}; \hat{Y} = \frac{(\hat{a} - \hat{a}^\dagger)}{2i} \quad (4.17)$$

There are a few advantages on using these operators. First, the Hamiltonian becomes

$$\hat{H} = \hbar\omega(\hat{n} + 1/2) = \hbar\omega(\hat{X}^2 + \hat{Y}^2). \quad (4.18)$$

which means that the zero-point energy is now connected with the quadrature variances of the vacuum state. Besides, the two quadrature operators do not commute,

$$[\hat{X}, \hat{Y}] = \frac{i}{2} \quad (4.19)$$

which leads to a Heisenberg uncertainty relation for the quadrature variances defined as

$$(\Delta \hat{X})^2 (\Delta \hat{Y})^2 \geq \frac{1}{16} \quad (4.20)$$

Applying the vacuum state is trivial to demonstrate that it is an example of a minimum uncertainty state with equal uncertainties in each quadrature, i.e.

$$(\Delta \hat{X})^2 = (\Delta \hat{Y})^2 = \frac{1}{4} \quad (4.21)$$

which saturates the Heisenberg uncertainty principle.

Finally, you can also define the quadrature operators in the generalized form

$$\hat{X}(\theta) = \frac{\hat{a}e^{i\theta} + \hat{a}^\dagger e^{-i\theta}}{2}; \hat{Y}(\theta) = \frac{(\hat{a}e^{i\theta} - \hat{a}^\dagger e^{-i\theta})}{2i} \quad (4.22)$$

Heisenberg uncertainty relation: If $\hat{C} = [\hat{A}, \hat{B}]$ then $(\Delta A)^2 (\Delta B)^2 \geq \frac{1}{4} |\langle C \rangle|^2$.

Exercise 4. Compute the variance of the quadrature operators for the vacuum state and show that this state minimizes the Heisenberg uncertainty principle.

Exercise 5. Prove the Hamiltonian form for the quadrature operators and establish the connection between the zero point energy of the vacuum state and the variance of the quadratures.

4.2 A Quantum Model for the Michelson Interferometer

Having introduced the necessary tools we will now describe the Michelson interferometer in the quantum picture, utilizing for this the matrix formalism. Using the notation introduced in Figure 17 we have that annihilation operators after the first beam splitter are given by

$$\begin{bmatrix} \hat{a}_3 \\ \hat{a}_4 \end{bmatrix} = \frac{1}{\sqrt{2}} \begin{bmatrix} e^{i\frac{2\pi L}{\lambda}} & 0 \\ 0 & 1 \end{bmatrix} \begin{bmatrix} 1 & i \\ i & 1 \end{bmatrix} \begin{bmatrix} \hat{a}_1 \\ \hat{a}_2 \end{bmatrix} \\ = \frac{1}{\sqrt{2}} \begin{bmatrix} e^{i\phi/2}(\hat{a}_1 + i\hat{a}_2) \\ i\hat{a}_1 + \hat{a}_2 \end{bmatrix} \quad (4.23)$$

and at the output ports

$$\begin{bmatrix} \hat{a}_5 \\ \hat{a}_6 \end{bmatrix} = \frac{1}{2} \begin{bmatrix} 1 & i \\ i & 1 \end{bmatrix} \begin{bmatrix} e^{i\frac{2\pi L}{\lambda}} & 0 \\ 0 & 1 \end{bmatrix} \begin{bmatrix} e^{i\frac{2\pi L}{\lambda}} & 0 \\ 0 & 1 \end{bmatrix} \begin{bmatrix} 1 & i \\ i & 1 \end{bmatrix} \begin{bmatrix} \hat{a}_1 \\ \hat{a}_2 \end{bmatrix} \\ = \frac{1}{2} \begin{bmatrix} (e^{i\phi} - 1)\hat{a}_1 + i(e^{i\phi} + 1)\hat{a}_2 \\ i(e^{i\phi} + 1)\hat{a}_1 + (1 - e^{i\phi})\hat{a}_2 \end{bmatrix} \quad (4.24)$$

. In this form, we note that the beam splitter mix the states in an uneven form, meaning that results both at the mirrors and at the output ports will be different from the quantum perspective levels. Indeed, the presence of fluctuations of the ground state will require to keep track of the \hat{a}_2 terms even when the state entering port 2 is the vacuum state $|0\rangle_2$. This is different from the classical case where we drop the $E_2 = 0$ terms and will lead to very distinct results.

4.2.1 Radiation Pressure

The radiation pressure is connected to the fluctuation of the force acting on the mirrors. In this way, we can say that the force difference will be connected to the fluctuation of the number of photons reaching the two mirrors, which means that the radiation pressure will be proportional to $\hat{n}_4 - \hat{n}_3$ which leads

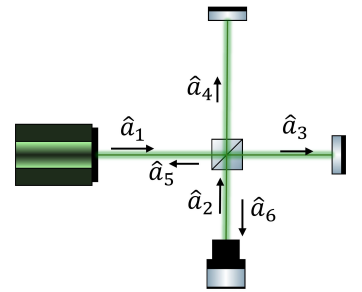


Figure 17. Michelson interferometer in operator picture.

to

$$\begin{aligned}\hat{P}_{rad} &\propto \hat{n}_4 - \hat{n}_3 = \hat{a}_4^\dagger \hat{a}_4 - \hat{a}_3^\dagger \hat{a}_3 \\ &= \frac{i}{2} (\hat{a}_2 \hat{a}_1^\dagger - \hat{a}_2^\dagger \hat{a}_1)\end{aligned}\quad (4.25)$$

Using a coherent state $|\beta\rangle_1$ with $\beta = |\beta|e^{i\theta}$ we have

$$\hat{P}_{rad} \propto |\beta| \hat{Y}_2(\pi/2 - \theta) \quad (4.26)$$

meaning that the fluctuations of the radiation pressure are connected with the fluctuations of the quadrature operator \hat{Y} , and thus, with the zero point energy of the electromagnetic field. Radiation pressure can then be understood as an effect that **occurs due to the beating of the coherent field and the vacuum entering port 2**. Besides, it is proportional to the variance $Var(\hat{Y}_2(\pi/2 - \theta))$, which for the vacuum state $|0\rangle_2$ is $1/4$, giving

$$u_{\Delta L}^{RPN} \propto \sqrt{Var(\hat{P}_{rad})} = |\beta| \sqrt{Var(\hat{Y}_2(\pi/2 - \theta))} = \frac{1}{2} |\beta| = \frac{1}{2} \sqrt{\frac{P}{\hbar\omega}} \quad (4.27)$$

4.2.2 Shot Noise

Where we utilize the definition $\frac{P}{\hbar\omega} = \bar{n}_{photons} = \langle \beta | \hat{n} | \beta \rangle = |\beta|^2$

For computing the shot noise we first compute the power at the output port 6, proportional to the mean value of the number operator \hat{n}_6 , i.e.

$$\begin{aligned}\hat{P}_6 &\propto \hat{a}_6^\dagger \hat{a}_6 = \frac{1}{4} (\gamma^* \hat{a}_1^\dagger + \sigma^* \hat{a}_2^\dagger)(\gamma \hat{a}_1 + \sigma \hat{a}_2) \\ &= \frac{1}{4} (|\gamma|^2 \hat{a}_1^\dagger \hat{a}_1 + |\sigma|^2 \hat{a}_2^\dagger \hat{a}_2 + \gamma \sigma^* \hat{a}_2^\dagger \hat{a}_1 + \gamma^* \sigma \hat{a}_1^\dagger \hat{a}_2),\end{aligned}\quad (4.28)$$

where we defined $\gamma = e^{i\phi} + 1$ and $\sigma = 1 - e^{i\phi}$. Taking the mean for the state $|\psi\rangle = |\beta\rangle_1 |0\rangle_2$ we get

$$\bar{P}_6 \propto \langle \psi | \hat{n}_6 | \psi \rangle = \frac{1}{4} |\beta|^2 |\gamma|^2. \quad (4.29)$$

Now to compute the noise, one should look at the variance of the operator \hat{P}_6 looking at its definition it is trivial to demonstrate that for state $|\psi\rangle = |\beta\rangle_1 |0\rangle_2$ we have

$$\begin{aligned}Var(\hat{P}_6) &\propto Var(\hat{n}_6) = \frac{1}{16} (|\gamma|^4 Var(\hat{n}_1) + |\sigma|^4 Var(\hat{n}_2) + 4|\sigma|^2 |\gamma|^2 |\beta|^2 Var(\hat{X}_2)) \\ &= \frac{1}{16} (|\gamma|^4 |\beta|^2 + 4|\gamma|^2 |\sigma|^2 |\beta|^2 Var(\hat{X}_2))\end{aligned}\quad (4.30)$$

where we utilize the fact that the variance of the number operator for a Fock state is 0 and for a coherent state is $|\beta|^2$.

Before ending the discussion it is important to make three remarks:

- First, we see again a relation between noise and fluctuations of vacuum, now in the form of the other quadrature operator \hat{X}_2 . This mathematical formalism was first proposed by Caves in 1981, with the conclusion that the quantum noise at the readout is also related to the quantum vacuum state entering port 2.
- It is trivial to demonstrate that

$$\begin{aligned} |\gamma|^2 &= 2(1 + \cos(\phi)) \\ |\sigma|^2 &= 2(1 - \cos(\phi)) \end{aligned} \quad (4.31)$$

and considering the case of vacuum state, i.e. $\text{Var}(\hat{X}_2) = 1/4$ this means that

$$\text{Var}(\hat{P}_6) = \frac{|\beta|^2}{4}(1 + \cos(\phi)). \quad (4.32)$$

If we compute the signal-to-noise ratio for a small gravitational wave producing ΔL and considering $\phi = \frac{4\pi\Delta L}{\lambda} + \phi_0$, we can take the signal as a small perturbation to the power of the port 6

$$\Delta \bar{P}_6 = \frac{\partial \bar{P}_6}{\partial \Delta L} \Delta L \propto \frac{2|\beta|^2 \pi}{\lambda} \sin(\phi_0) \Delta L \quad (4.33)$$

and the noise as the root square of the variance, meaning that

$$\text{SNR} \propto \frac{\Delta \bar{P}_6}{\sqrt{\text{Var}(\hat{P}_6)}} = \frac{4|\beta|^2 \pi \sin(\phi_0) \Delta L}{\lambda |\beta| \sqrt{1 + \cos(\phi_0)}} = \frac{2|\beta| \pi \sin(\phi_0)}{\lambda \cos(\phi_0/2)} \Delta L. \quad (4.34)$$

By plotting the SNR (see Figure 18) it can be seen that it attains its maximum at $\phi_0 = (2m + 1)\pi$, i.e. **at the dark fringe**, proving our empirical statement introduced before in this chapter.

- Finally, by following the same methodology as before, we can compute the maximum uncertainty related with the shot noise as

$$u_{\Delta L}^{SN} = \frac{\sqrt{\text{Var}(\hat{P}_6)}}{\frac{\partial \bar{P}_6}{\partial \Delta L}} = \frac{\lambda}{2\pi|\beta|} = c\sqrt{\frac{\hbar}{2\omega P}} \quad (4.35)$$

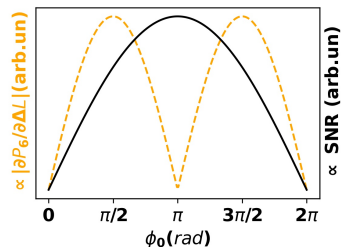


Figure 18. In LIGO, the operation point is the dark fringe and not the quadrature point, and that is due to the fact that the SNR for the shot noise contribution has a minimum in that region.

4.3 Squeezed States and Reduction of noise

Recovering the uncertainty relation for the quadrature operators we see that we have a fundamental limit. Yet, it still presents some degree of versatility:

we can for example increase the variance in the direction of \hat{X} while decreasing in the direction of \hat{Y} . Taking into consideration our picture for noises, this would mean to reduce the shot-noise at the expense of increasing the radiation pressure noise, which depending on the zone we are working can lead to higher sensitivities. This is the concept behind **vacuum squeezing**.

In the context of quantum optics, squeezing involves manipulating the quantum state of light to reduce noise in one observable at the expense of increased noise in its conjugate variable, respecting the Heisenberg Uncertainty Principle. The process is typically realized by using a nonlinear optical medium to perform parametric down-conversion (e.g. pumping a BBO crystal with double the frequency, creating pairs of photons at half of the frequency) or four-wave mixing(see Figure 19). For example, a squeezing interaction can arise from the Hamiltonian written as

$$\hat{H}_s = i\hbar\chi(\hat{a}^{\dagger 2}\hat{b} - \hat{a}^2\hat{b}^\dagger) \quad (4.36)$$

where \hat{a} and \hat{a}^\dagger are operators for the field that exits the crystal at frequency $\omega_2 = 2\omega_1$, whereas \hat{b} and \hat{b}^\dagger are operators for the field entering the crystal at frequency ω_1 . Also, χ is a parameter related to the nonlinear properties of the medium and intensity of the pump beam, controlling **the strength of the squeezing interaction**.

It can be noted that the form of the Hamiltonian means that one photon at frequency ω_1 is annihilated/created leading to creation/annihilation of two photons at frequency ω_2 . Beside, if we consider that we have an input state

$$|\psi_{in}\rangle = |\xi\rangle_1|0\rangle_2 \quad (4.37)$$

meaning that at the entrance of the crystal, we have a coherent state (i.e. a laser beam) on the field oscillating at ω_1 and a vacuum state on the field oscillating at ω_2 , we can get a reduced Hamiltonian in the state space of ω_2 given by

$$\hat{H}_s = i\hbar\chi(\xi\hat{a}^{\dagger 2} - \xi^*\hat{a}^2) \quad (4.38)$$

Taking the Schrödinger equation

$$i\hbar\partial_t|\psi\rangle_2 = \hat{H}_s|\psi_{in}\rangle_2 \quad (4.39)$$

and the formal

$$|\psi_{out}\rangle_2 = \exp\left(\frac{\hat{H}_s t}{i\hbar}\right)|\psi_{in}\rangle_2 \quad (4.40)$$

we get

$$|\psi_{out}\rangle_2 = \exp\left(\chi t(\xi\hat{a}^{\dagger 2} - \xi^*\hat{a}^2)\right)|\psi_{in}\rangle_2 = \hat{S}(r)|\psi_{in}\rangle_2 \quad (4.41)$$

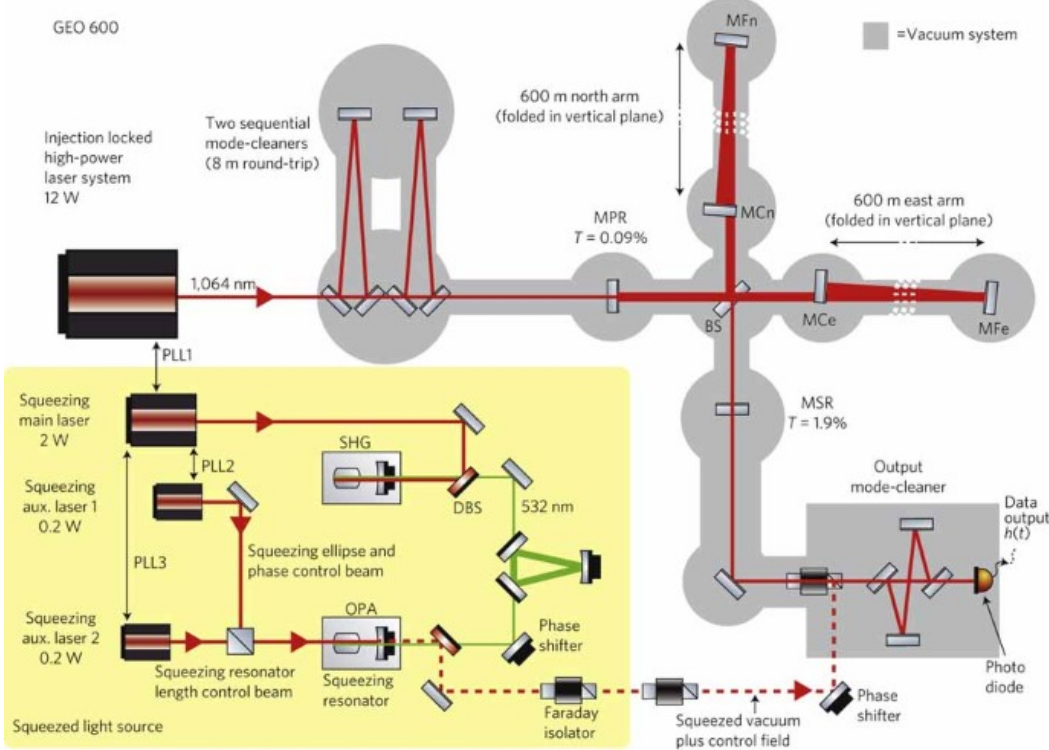


Figure 19. Squeezing module in LIGO. First, the coherent state from the laser is doubled in frequency using second harmonic generation in a first nonlinear crystal (green path), which is retrieved back again to the original frequency using four-wave mixing in the second crystal. Note that a squeezed state is not a vacuum state, but a state that is created from vacuum for which there are photon pairs with some degree of correlations.

where the **squeezing operator** can be

$$\hat{S}(r) = \exp\left(\frac{1}{2}(r\hat{a}^{\dagger 2} - r^*\hat{a}^2)\right) \quad (4.42)$$

with $r = 2\chi|\xi|t$.

4.3.1 Surpassing the SQL using squeezing

In the context of our case study, we can proceed with our analysis by applying the squeezing operator to the vacuum state, i.e.

$$|r\rangle = \hat{S}(r)|0\rangle_2 \quad (4.43)$$

where $|r\rangle$ is now the squeezed vacuum state. For the sake of simplicity, we will consider r as a real value from now on.

It can be shown that the squeezing operation transforms the annihilation

and creation operators as

$$\hat{S}^\dagger(r)\hat{a}\hat{S}(r) = \hat{a} \cosh(r) - \hat{a}^\dagger \sinh(r) \quad (4.44)$$

$$\hat{S}^\dagger(r)\hat{a}^\dagger\hat{S}(r) = \hat{a}^\dagger \cosh(r) - \hat{a} \sinh(r) \quad (4.45)$$

leading to the transformation of the quadrature operators

$$\hat{X}' = \hat{S}^\dagger(r)\hat{X}\hat{S}(r) = e^{-r}\hat{X} \quad (4.46)$$

and

$$\hat{Y}' = \hat{S}^\dagger(r)\hat{Y}\hat{S}(r) = e^r\hat{Y} \quad (4.47)$$

It is then straightforward to compute the squeezed variances

$$Var(\hat{X}') = e^{-2r}Var(\hat{X}) = \frac{1}{2}e^{-2r}, \quad (4.48)$$

and

$$Var(\hat{Y}') = e^{2r}Var(\hat{Y}) = \frac{1}{2}e^{2r}. \quad (4.49)$$

This means that the squeezing Hamiltonian generates correlations that effectively squeeze the quantum state in the phase space, reducing uncertainty in one of the directions at the expense of the other.

Putting this result against the work we have done so far, **this demonstrates that a squeezing process allows to enhance the precision of the measurement of gravitational waves, surpassing the standard quantum limit baseline introduced before.** Note however that this is done within the hard boundaries defined by the Heisenberg limit and in a **broader perspective** means that the use of **squeezing may help improve the precision of sensors beyond the limits imposed by quantum fluctuations.**

Exercise 6. Using the modified Baker-Campbell-Hausdorff formula

$$e^{\hat{A}}\hat{B}e^{-\hat{A}} = \hat{B} + \frac{1}{2} [\hat{A}, \hat{B}] + \frac{1}{2!} [\hat{A}, [\hat{A}, \hat{B}]] + \dots \quad (4.50)$$

prove that for a real-valued r , the annihilation operator is transformed by the squeezing process as

$$\hat{S}^\dagger(\xi)\hat{a}\hat{S}(\xi) = \hat{a} \cosh(r) - \hat{a}^\dagger \sinh(r). \quad (4.51)$$

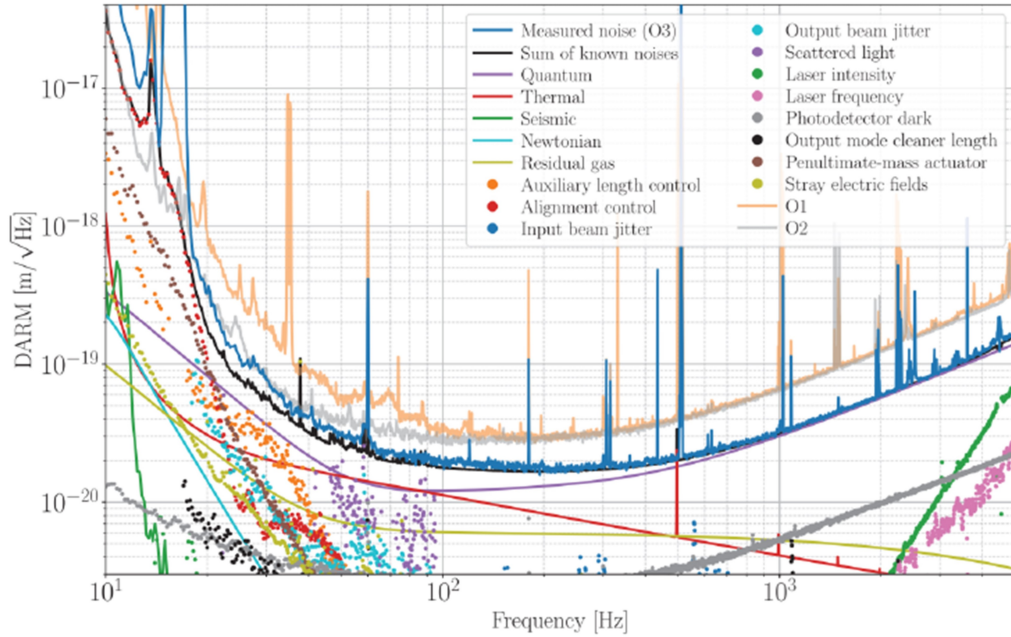


Figure 20. Squeezing noise reduction may be observed in the experimentally calculated noise for LIGO, in particular from O1 and O2 observation seasons to O3.

Optical state Phase Space: A common and intuitive representation of an optical state comes in the form of the phase space defined using the quadrature operators. The precise definition involves Wigner function formalism but in simple terms, the idea is to represent each state as a probability density function centered in the mean value of quadrature operators \hat{X} and \hat{Y} and with widths that vary depending on the variances $Var(\hat{X})$ and $Var(\hat{Y})$, which better illustrates the concept of state squeezing.

Note the connection of these with the position and momentum operators of a harmonic oscillator

5 Concluding Remarks

LIGO has marked a revolutionary milestone in the field of physics, enabling the ground-breaking detection of gravitational waves that not only confirmed key predictions of Einstein's General Theory of Relativity but also pave for an entirely new way of observing the universe. Yet, achieving this breakthrough required the development of innovative engineering solutions and state-of-the-art technologies.

Indeed, the extreme sensitivity needed to detect gravitational waves first required enhancements at the engineering and technological levels. However, this quest for ultra-sensitivity also brought to light the fundamental barriers imposed by the quantum nature of light. With the increase of LIGO sensitiv-

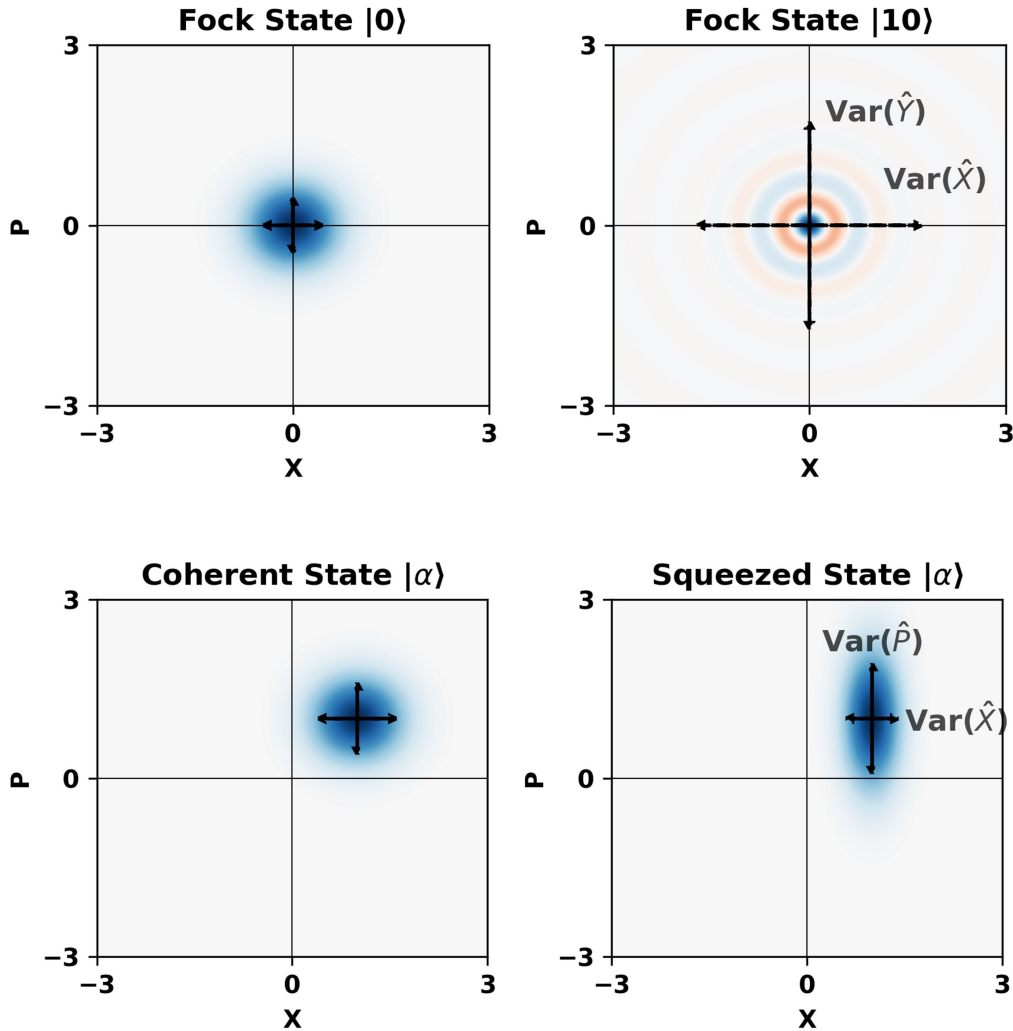


Figure 21. Examples of the representation of fock, coherent, and squeezed states on the Optical Phase Space.

ity, it became evident that classical sources of noise could be mitigated only up to a point: the **standard quantum limit**, related to quantum fluctuations and influencing both the power detected - **shot noise** - but also the optical force on the mirrors - **radiation pressure**.

In this chapter, we explored these problems in depth, overviewing LIGO construction and analyzing in detail the noise origins and mitigation strategies. In particular, in the last part, by modeling the interferometer within a quantum framework, we identified that the noise results from the interaction between the coherent laser light and the vacuum state of the electromagnetic field entering the unused port of the beamsplitter. The interference of vacuum fluctuations and the main laser leads to uncertainties in the phase and amplitude measurements by perturbing the radiation pressure and shot noise at the detector.

Finally, leveraging on the Heisenberg uncertainty principle and introducing the concept of squeezed states of light, we show that through nonlinear optics it is possible to manipulate the vacuum state achieving a squeezing that can reduce the uncertainty in one observable (such as phase) at the expense of increased uncertainty in the conjugate observable (such as amplitude). This technique effectively redistributes the quantum noise, allowing for a reduction in the noise component. Thus, we show that through the use of quantum formalism is not only possible to understand the true origin of the noise but also to present strategies to mitigate it, paving for sensors that are able to operate beyond the standard quantum limit

A final note on the topic regards the frequency dependency of the noise in LIGO. The squeezed vacuum we described does not depend on the frequency, meaning that it has the same impact across all frequencies. However, to enhance detection capabilities, it would be beneficial to create a state with quadrature variances that vary with the frequency, e.g. transitioning from phase squeezing at higher frequencies to amplitude squeezing at lower frequencies. This frequency-dependent squeezing can be done experimentally by adding a frequency-dependent delay, accomplished by reflecting the phase-squeezed vacuum off a long optical cavity. This method optimizes the squeezing effect across different frequencies, improving the sensitivity of LIGO measurements.